Review of Scientific Instruments

RESEARCH ARTICLE | JUNE 23 2023

Detection of electromagnetic phase transitions using a helical cavity susceptometer

Pavel N. Lapa ; George Kassabian ; Ali C. Basaran ; Ivan K. Schuller

Rev Sci Instrum 94, 064710 (2023)
https://doi.org/10.1063/5.0136523

AIP Publishing

Review of Scientific Instruments ARTICLE scitation.org/journal/rsi

Detection of electromagnetic phase transitions using a helical cavity susceptometer

Cite as: Rev. Sci. Instrum. 94, 064710 (2023); doi: 10.1063/5.0136523
Submitted: 26 November 2022 • Accepted: 5 June 2023 •
Published Online: 23 June 2023

Pavel N. Lapa,[a] George Kassabian, Ali C. Basaran, and Ivan K. Schuller

AFFILIATIONS

Department of Physics and Center for Advanced Nanoscience, University of California San Diego, La Jolla, California 92093, USA

[a]Author to whom correspondence should be addressed: plapa@physics.ucsd.edu

ABSTRACT

Fast and sensitive phase transition detection is one of the most important requirements for new material synthesis and characterization. For solid-state samples, microwave absorption techniques can be employed for detecting phase transitions because it simultaneously monitors changes in electronic and magnetic properties. However, microwave absorption techniques require expensive high-frequency microwave equipment and bulky hollow cavities. Due to size limitations in conventional instruments, it is challenging to implement these cavities inside a laboratory cryostat. In this work, we designed and built a susceptometer that consists of a small helical cavity embedded into a custom insert of a commercial cryostat. This cavity resonator operated at sub-GHz frequencies is extremely sensitive to changes in material parameters, such as electrical conductivity, magnetization, and electric and magnetic susceptibilities. To demonstrate its operation, we detected superconducting phase transition in Nb and $YBa_2Cu_3O_{7-\delta}$, metal–insulator transitions in V_2O_3, ferromagnetic transition in Gd, and magnetic field induced transformation in meta magnetic NiCoMnIn single crystals. This high sensitivity apparatus allows the detection of trace amounts of materials (10^{-9}-cc) undergoing an electromagnetic transition in a very broad temperature (2–400 K) and magnetic field (up to 90 kOe) ranges.

I. INTRODUCTION

Phase transitions observed in micro[1] and macro[2] systems are interesting for the synthesis of novel materials and for searches for new electromagnetic phases. The unique change in properties occurring at phase transitions allows the classification and detection of materials based on their physical properties, including ferromagnets, ferroelectrics, and superconductors. Precise detection of electromagnetic phase transitions can be extremely challenging, requiring specialized equipment and techniques. In most cases, an inevitable inhomogeneity in the samples must be considered; for example, a mixture of substances showing the same type of phase transition but under different conditions can coexist. Furthermore, a phase transition in a solid-state matter results in various structural, electronic, and magnetic states. Typical measurements, such as x-ray diffractometry, electronic transport, and magnetometry, are usually sensitive to only one of these states. On the other hand, microwave absorption measurements[3] can be simultaneously sensitive to the modification of electronic and magnetic properties of materials. A resonant microwave-absorption approach is notoriously sensitive, which allows for studying phase transitions of tiny amounts of material.[1,2] This unique feature makes the microwave absorption techniques particularly attractive for detecting phase transitions in various sample sizes and shapes.

The resonant microwave-absorption technique requires large cavities of the order of cm sizes to satisfy resonance conditions and needs to be combined with a flow cryostat to control broader temperature ranges. To the first approximation, the eigenmode resonant frequency of a hollow resonant cavity, f_{res}, is inversely proportional to its size; for example, for a hollow cylindrical cavity with a diameter of 13 mm and a length of 26.3 mm, the resonant frequency of the TE_{011} mode is 15.2 GHz. Such high-frequency cavity operation requires relatively expensive, in many cases highly specialized, excitation and detection equipment embedded in a complicated auxiliary thermal and magnetic field environment. On the other hand, most commercial cryostats that provide cryogenic temperatures in high magnetic fields have important size limitations. Thus, the development of a high frequency detection system that can easily be incorporated into a commercial cryostat is desirable.

In this study, we have designed and fabricated a versatile "helical cavity (HC) susceptometer," which consists of a cylindrical HC mounted on a custom-made attachment of a commercial cryostat. Despite its small size, the HC can be excited by a sub-GHz RF generator.[3] Additionally, a custom phase-locked loop (PLL) has

been implemented using a combination of common electronics and device control software. We showed that PLL and the high Q-factor enable monitoring of small changes in conductivity and electrical and magnetic permeability with very high sensitivity. We show that the HC susceptometer is extremely useful for the fast detection of electromagnetic phase transitions in different materials in the temperature range of 2–400 K and magnetic fields up to 90 kOe. Thus, the main advantage of the apparatus in comparison to other instruments is that it can be used for fast, sensitive, and selective analysis of various phase transitions in inhomogeneous or mixed-phase samples. Additionally, the design enables easy integration into existing laboratory cryostats and advances the modification of instrument-control algorithms to meet the requirements of custom experiments.

II. APPARATUS DESIGN

An HC resonator can be considered a hybrid between a hollow RF cavity and a coaxial resonator.[4] Such resonators have broad applications in high-frequency communication[3,5,6] as filters and amplifiers. HC resonators are also used in research for ion-beam acceleration,[7] measurement of dielectric properties of materials, and surface conductivity.[8–10] The structure of HC used in the apparatus is shown in Figs. 1(a) and 1(b). It consists of a cylindrical cavity enclosing a helical wire, one end of which is connected to the wall of the cavity [Fig. 1(a)], a top lid with a thin glass sample container, and a base lid carrying the helix, small excitation and detection coils connecting to the corresponding micro-miniature push-on RF ports mounted at the bottom [Figs. 1(b) and 1(c)]. The reference port is directly wired to the excitation port inside the cavity [Fig. 1(b)]. The cavity body is machined from oxygen-free C110 copper. The helix made of pure copper 20 gauge wire has 8 turns. The diameter of the helix is 7 mm, and the distance between turns is 1.3 mm. The excitation and detection coils have two 1.5-mm diameter turns. The cavity is connected to the base of the cryostat insert made of G10 fiberglass laminate, which is widely used in cryogenic applications [Figs. 1(c) and 1(d)]. The insert rod made of an 8-mm carbon fiber tube contains four isolation baffles. Three 1.13-mm RF cables with identical lengths connect the cavity with the top of the insert, where four vacuum-sealed SMA (SubMiniature version A) connectors are mounted. This insert is designed to be compatible with the Quantum Design PPMS system and is easily adaptable to other similar cryostats. A calibrated Cernox temperature sensor attached to the cavity wall from the outside is connected to the cryostat socket puck and allows precise temperature tracing of the cavity with a sample [Fig. 1(c)].

The cavity is excited by an Agilent E4422B generator. The detection and reference output are analyzed using an amplitude and phase detection module based on the AD8302 microchip. The analog voltage from the detector passes through a low pass filter, which is amplified twice and read by a 16-bit analog-to-digital converter [bottom schematics at Fig. 1(a)]. Figure 1(e) shows the frequency sweep of AC-voltage amplitude on the detection coil and its phase with respect to the reference signal near the fundamental-mode frequency, f_{res} = 570 MHz. This fundamental-mode frequency is much lower than that for a hollow cavity of this size (15.2 GHz). At resonance, the amplitude of the transmitted signal voltage increases more than four times. Based on these data, the cavity Q-factor is

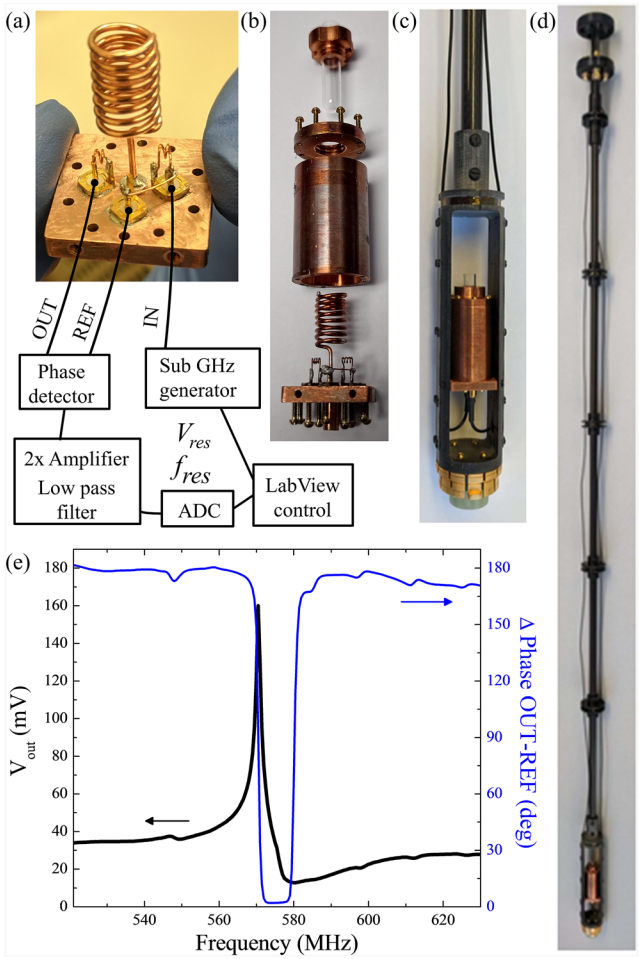

FIG. 1. (a) Schematics of the HC design and block diagram of electronics and (b) components of the disassembled HC [from top to bottom: sample tube, top lid, cylindrical wall, and a base containing helix, excitation (IN)/pick-up (OUT) coils]. The central pin of the reference (REF) connector is soldered to the central pin of the excitation connector. (c) The assembled HC is installed on the cryostat insert (d). (e) Examples of frequency dependences of transmitted voltage amplitude, V_{OUT} (left scale), and phase shift between OUT and REF (right scale).

equal to 300. The signal phase changes smoothly from 180° to almost 0° in the vicinity of f_{res}, whereas, at f_{res}, the phase is 90°. Note that the length of the detection and reference cables are intentionally chosen to be the same, so their properties change synchronously with temperature since they are subjected to the same environmental conditions inside the cryostat. This ensures that there is no frequency-dependent phase change. As a consequence, a potential oscillatory component of the transmitted voltage amplitude and phase with frequency is absent, i.e., there are no significant changes in the transmitted signal phase and amplitude outside the resonant region [Fig. 1(e)]. This helps greatly the detection of the resonance and makes measured parameters more reliable.

Once a sample is placed into the HC and the f_{res} is determined, two measurements are possible using the HC susceptometer: frequency-locked loop (FLL) and phase-locked loop (PLL). For the

FLL approach, the frequency of excitation RF signal is kept constant and equal to f_{res} while recording the detection-coil AC voltage amplitude, V_{res}, and its phase as a function of temperature or magnetic field. FLL can only be used for magnetic field or narrow-range temperature scans. If the temperature varies in a wide range, parameters of the HC (conductivity) and RF cables (dielectric constant and losses) change significantly, which results in the cavity detuning and, hence, a loss of susceptometer sensitivity. In contrast, the PLL approach provides high sensitivity in a full range of temperatures and magnetic fields, which is achieved by constant tuning of excitation frequency to maintain a 90° phase difference. This ensures that the cavity always operates at the resonant frequency (S.1 in the supplementary material). For the HC susceptometer in this work, the PLL is realized using a custom LabView software, which adjusts the generator frequency to maintain a 90° phase difference. As a first step of the PLL, the frequency change is calculated from the frequency dependence of the phase [blue curve in Fig. 1(e)]. For each subsequent step, the coefficient of frequency change is updated based on the phase value obtained in the previous step. To avoid an oscillation of the PLL, which may occur due to overshooting and a slow relaxation caused by undershooting, the PLL coefficient is decreased or increased by 5% when the phase overshoots or undershoots, respectively. Figure S1 in the supplementary material shows a comparison of PLL and FLL measurements for the same sample, whereas the data in Fig. S2 demonstrate the FLL scan for the Nb chip and unambiguously exhibit the effect of cavity detuning in a wide temperature scan range.

III. EXPERIMENTAL RESULTS

The potential of this equipment is shown by performing measurements in a series of well-known situations, including phase transitions, such as superconducting, metal–insulator, or ferromagnetic, as a function of magnetic field and temperature. All the data presented below were obtained using the PLL approach.

A. Superconducting transition in Nb and $YBa_2Cu_3O_{7-\delta}$ (YBCO)

Figure 2 shows temperature dependences of the resonant voltage V_{res} and frequency f_{res} for a 3 mg Nb chip. The data were obtained at different applied magnetic fields ranging from 0 to 90 kOe by continuously sweeping the temperature from 12 to 2 K with a 0.5 K/min rate. In the absence of a magnetic field, V_{res} and f_{res} show an abrupt increase at 8.9 K.[11] This transition temperature is about 0.3 K lower than the expected bulk Nb superconducting transition temperature of 9.25 K, which was detected for the same sample using QD DynaCool vibrational sample magnetometer (VSM) (see Fig. S3 in the supplementary material). The slightly lower superconducting temperature detected with the HC susceptometer may be due to a difference between the temperature reading by the cavity of the thermometer and the actual sample temperature or due to the natural oxidation that may occur on the surface of the sample. Further evidence for the first case is proven by the 0.15 K hysteresis depending on the temperature sweep direction (inset in Fig. 2). Additionally, as it is discussed in the supplementary material, the HC

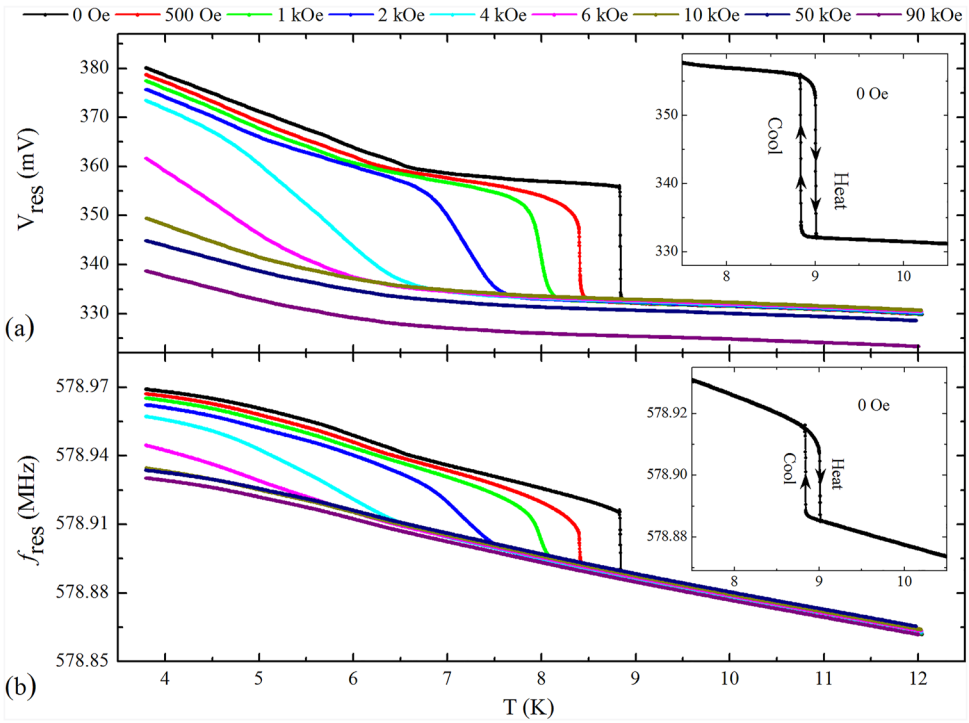

FIG. 2. (a) Temperature dependences of the resonant voltage of the transmitted RF signal, V_{res}, and (b) resonant frequency, f_{res}, for the cavity with 3-mg Nb sample measured in magnetic fields ranging from 0 to 90 kOe. Insets show the zero-magnetic-field curves (black) in the vicinity of the superconducting transition.

susceptometer is sensitive to changes in material properties localized within the skin depth from the surface, whereas the VSM probes the entire sample volume. Thus, partial oxidation of the Nb chip's surface may explain the reduction of the nominal Nb superconducting temperature and, thus, may be responsible for the temperature difference. According to Fig. 2, an increase in the applied magnetic field produces a shift of V_{res} and f_{res} to lower temperatures and smears the transition.

The temperature dependences of V_{res} and f_{res} for a 100 nm YBCO film (2×4 mm^2) measured in zero fields (black curve) and 90 kOe magnetic field (red curve) are shown in Figs. 3(a) and 3(b). Overall, the dependencies look similar to those obtained for the Nb chip. V_{res} and f_{res} increase at the SC transitions of 84 and 82 K for 0 and 90 kOe applied magnetic fields, respectively. However, in contrast to the Nb chip, these transitions are less abrupt: the significant variation of V_{res} and f_{res} completes at 82 and 73 K for 0 and 90 kOe applied fields, respectively. Moreover, V_{res} exhibits a dip at the beginning of the transition, which slightly rises and reaches a plateau. Additionally, f_{res} starts decreasing below 55 K. The resonance below 20 K becomes unstable for the YBCO sample. All these sample-specific features might be related to mechanisms that appear at low temperatures in high-temperature superconducting thin films, such as vortex motion and pinning or weak links due to granularity.[12–14] Additionally, Fig. 3(c) shows the magnetic field dependence of V_{res} measured at 50 K when YBCO is in the superconducting state. The instability observed in the low magnetic field may be further evidence of the complex vortex behavior affecting microwave dissipation, which can be further studied by such HC susceptometers.

From the data presented above, we can calculate the sensitivity of detecting a SC transition using the helical cavity susceptometer. Considering that the film's volume is about 10^{-6} cc and the measurements noise of V_{res} and f_{res} is on the level of 0.1%., the sensitivity of these measurements is of the order of 10^{-9} cc superconducting volume.

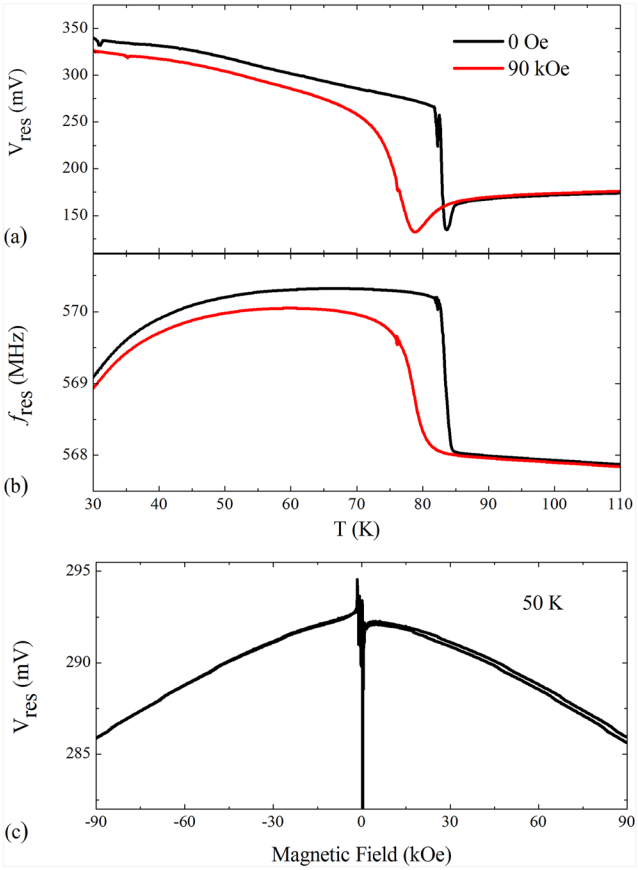

FIG. 3. (a) Temperature dependences of the resonant voltage of the transmitted RF signal, V_{res}, and (b) resonant frequency, f_{res}, for the cavity with the YBCO film measured in 0-kOe (black curve) and 90-kOe (red curve) magnetic fields. (c) The magnetic field dependence of V_{res} was measured at 50 K.

B. Metal–insulator transition in V_2O_3

V_2O_3 is a classic example of a material that undergoes a metal–insulator transition. We grew a 100 nm V_2O_3 film (2×7 mm^2) on an Al_2O_3 substrate and measured the temperature-dependent resistance to relate it to the HC signal. The V_2O_3 film exhibits a six-order of-magnitude resistance change at the metal–insulator transition [Fig. 4(a)]. Metallic behavior, with a characteristic resistivity decrease with temperature decrease, was observed down to 182 K. Further decreasing temperature to 147 K, the resistivity shows a significant rise from 0.25 to 100 mOhm × cm, followed by a semiconductor-like rise of resistance below 147 K. The resistive transition exhibits a pronounced 8 K temperature hysteresis between cooling and heating curves.

The increase of the V_2O_3 resistivity during the transition yields a significant change in V_{res} and f_{res} for the cavity with the V_2O_3 sample.[15] While decreasing the temperature, V_{res} drops from 190 to 120 mV and then rises back to 220 mV. At the same time, f_{res} rises by 3 MHz during the transition into the insulating phase. The monotonic increase in V_{res} and f_{res} outside the transition temperature range is most probably due to the temperature variation of the HC conductivity. Both temperature dependences of V_{res} and f_{res} exhibit a hysteretic behavior similar to the resistivity. However, the width of the temperature hysteresis is about 13 K, which is slightly larger than the temperature hysteresis obtained in resistivity measurements.

C. Paramagnetic to ferromagnetic transition in Gd

Rare earth Gd undergoes a para-ferromagnetic transition at 293 K,[16,17] which enhances the real and imaginary parts of the AC magnetic susceptibility. In contrast to the paramagnetic phase, the susceptibility shows a strong nonlinear dependence on the magnetic field in the ferromagnetic phase. To monitor this magnetic transition in the HC setup, we used a 1 mg Gd sample and scanned the temperature across its phase transition. There is an apparent variation of V_{res} and f_{res} in the 280–300 K temperature range (Fig. 5) with low fields. In zero magnetic field, V_{res} demonstrates an onset of decrease at 298 K while the onset of f_{res} reduction appears at 10 K lower. An increased applied magnetic field to 500 and 1000 Oe results in suppression of V_{res} reduction, whereas the f_{res} onset shifts to higher temperatures. At 5 kOe applied field, which is sufficiently high for saturating magnetization of Gd in the ferromagnetic phase,

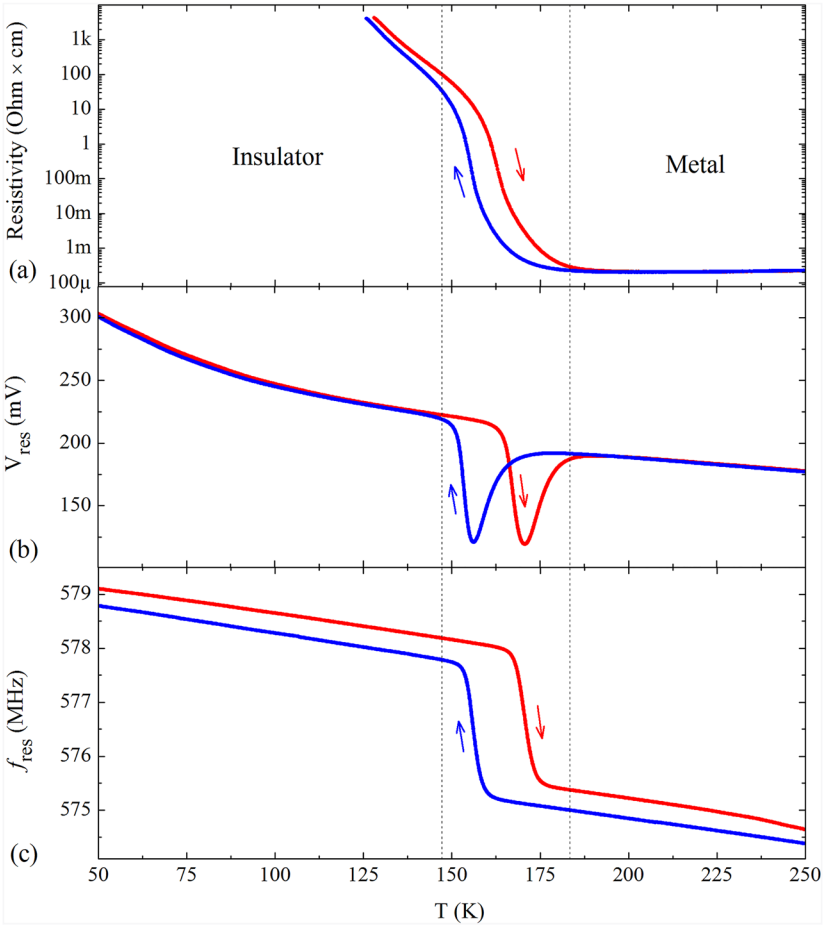

FIG. 4. (a) Change in resistivity for the 100-nm V_2O_3 film at the metal–insulator transition. The temperature depends on (b) the resonant voltage of the transmitted RF signal, V_{res}, and (c) the resonant frequency, f_{res}, for the cavity with the film. The data are obtained while cooling (blue curves) and heating (red curves). The vertical dashed lines show approximate temperatures at which the phase transformation starts and ends.

V_{res} and f_{res} demonstrate a linear rise with temperature, without the peculiarities in the 280–300 K temperature range (Fig. 5 green curve). This result suggests that the HC susceptometer can detect susceptibility changes at low fields across a paramagnetic to the ferromagnetic phase transition.

D. Magnetic field induced transformation in NiCoMnIn

Meta-magnetic shape memory alloy $Ni_{45}Co_5Mn_{36.7}In_{13.3}$ undergoes a martensitic transformation, which changes its magnetic moment and electrical conductivity.[18,19] In contrast to an ordinary paramagnetic to ferromagnetic transition, a high-temperature austenitic phase (above 295 K) is ferromagnetic, whereas a low-temperature martensitic phase (below 295 K) is weakly magnetic, which is often attributed to competing para magnetic–antiferromagnetic interactions.[20–22] Additionally, the phase transition can be controlled by a magnetic field, which leads to a magnetic field induced transformation (MFIT).[18] The MFIT is responsible for the appearance of peculiar lobes emerging in the high magnetic field on hysteresis loops measured at the transition temperature range.[19] Figures 6(a) and 6(b) show the temperature dependence of V_{res} and f_{res} for the HC with a 5 mg $Ni_{45}Co_5Mn_{36.7}In_{13.3}$ single crystal sample. For the dependencies measured in a 100 Oe magnetic field (black curve), V_{res} increases with decreasing temperature below 300 K when high magnetization austenite transforms to low magnetization martensite. At first glance, V_{res} increasing with decreasing temperature indicates that the system behavior is opposite to that of Gd. However, the nature of the transition itself is the opposite since, with decreasing temperature, Gd undergoes a transition to a high-magnetization ferromagnetic state while the $Ni_{45}Co_5Mn_{36.7}In_{13.3}$ transforms into a weakly magnetized martensitic phase. For 10 and 50 kOe applied magnetic fields, V_{res} exhibits a decrease in the middle of the transition, whereas V_{res} measured at 90 kOe magnetic field shows a step-like increase. Additionally, modification of f_{res} with temperature also strongly depends on the magnetic field. Namely,

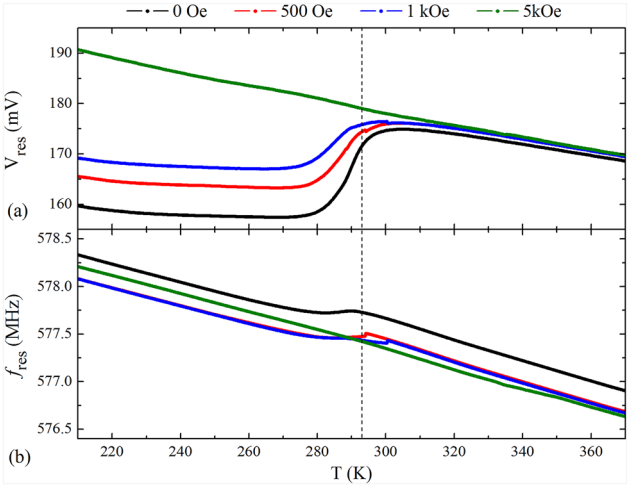

FIG. 5. Temperature dependences of (a) resonant voltage, V_{res}, and (b) resonant frequency, f_{res}, measured in the 0-Oe, 500-Oe, 1-kOe, and 5-kOe magnetic fields for the HC with 1-mg Gd sample undergoing paramagnetic–ferromagnetic phase transition at 293 K (the vertical dashed line).

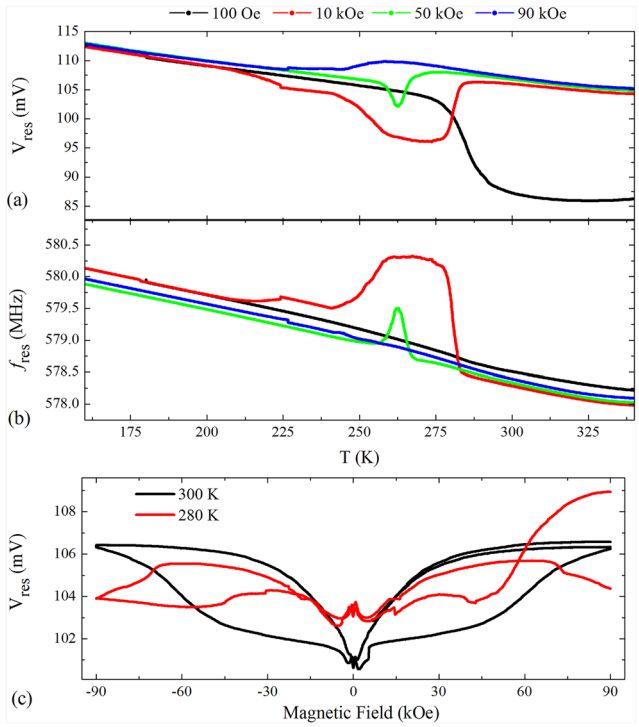

FIG. 6. Temperature dependences of (a) resonant voltage, V_{res}, and (b) resonant frequency, f_{res}, measured in different magnetic fields for the $Ni_{45}Co_5Mn_{36.7}In_{13.3}$ single crystal undergoing MFIT. (c) Hysteresis loops of V_{res} measured between 90 and 90 kOe at 300 K (black line) and 280 K (red line) evidence MFIT.

a substantial increase in f_{res} is observed only for the corresponding curves measured in the 10 and 50 kOe magnetic fields. This behavior can be attributed to a complex modification of susceptibility with MFIT. Figure 6(c) shows V_{res} loops measured as a function of the applied magnetic field swept between 90 and −90 kOe at 300 K (black line) and at 280 K (red line). The loops have pronounced hysteresis caused by MFIT. According to the hysteresis loops at different temperatures, MFIT starts in small magnetic fields at 300 K, while a substantial magnetic field (above 10 kOe) must be applied to initiate MFIT at 280 K.

IV. DISCUSSION

A theory providing a full description of microwave cavity absorption may be quite complicated due to the strong dependence on the cavity parameters and, especially, sample properties.[5,23–26] For the HC in this study, the sample is placed at the center of the coil where the RF magnetic field is maximal and aligned along the cavity axis. A simple model, which enables qualitative characterization of the sample absorption and yields a change in sample parameters at the phase transition, is given by the inductive-heating model.[27] The power dissipation density, P_d, can be expressed as

$$P_d \sim \frac{C\mu^2\sigma}{1 + C\mu^2\sigma^2}, \tag{1}$$

where μ and σ are the high-frequency magnetic permeability and conductivity, respectively, of a material, and C is a parameter that depends on the geometry of the sample and the excitation frequency.

According to Eq. (1), the cavity absorption increases with increasing μ. This explains the drop of V_{res} [Fig. 5(a)] for the HC with the Gd sample when it becomes ferromagnetic. The same explanation can be applied to the NiCoMnIn single crystal to justify the enhancement of V_{res} on the temperature dependence measured in 100 Oe [Fig. 6(a) black curve]; below 295 K, the material becomes paramagnetic, and μ decreases. For higher magnetic fields (10, 50, and 90 kOe) at temperatures at which MFIT takes place, μ is greatly enhanced since V_{res} is suppressed in the MFIT temperature range. The complex magnetization behavior is illustrated by the V_{res} hysteresis loops shown in Fig. 6(c). At 280 K, V_{res} starts to fall in magnetic fields exceeding 70 kOe. Surprisingly, substantial magnetic-field hysteresis is observed even at 300 K, which can be a sign of enhanced magnetic viscosity near the MFIT.

One of the interesting phenomena observed using the HC susceptometer is the "valley"-like suppression of V_{res} observed at the beginning of the superconducting transition for the YBCO film [Fig. 3(a)] and the valleys in the middle of the metal–insulator transition for the V_2O_3 film [Fig. 4(b)]. According to Eq. (1), the dependence of V_{res} on the conductivity is highly non-monotonic; a decrease in σ first leads to an enhancement of absorption until it reaches a maximum at $\sigma^* = 1/\sqrt{C}$ (assuming μ and ε are equal to 1). After that, a further decrease in σ leads to a reduction in absorption.[15] Thus, the microwave absorption reaches a maximum when the sample's conductivity is σ^*, where σ^* is defined by the sample geometry and excitation frequency. Since σ of the V_2O_3 film significantly changes at the metal–insulator transition, presumably reaching σ^* in the middle of the transition, which explains

the pronounced minimum of V_{res} during the transition. Although the morphology of the metal and insulating domains in V_2O_3 has previously been studied without high-frequency excitation and shown to be nearly the same during cooling and heating,[28] the eddy currents produced by the high-frequency electromagnetic field can cause local changes in the coexisting monoclinic and corundum phases that can increase absorption.[28,29] Moreover, the distribution and morphology of these fields during cooling and heating may be different, which explains the increase of thermal hysteresis on the temperature dependence of V_{res}.

Similarly to the V_2O_3 film, the occurrence of $\sigma = \sigma^*$ may explain the dip in the V_{res} observed at the beginning of the superconducting transition for the YBCO film. Interestingly, a microwave absorption peak was reported for another high-temperature $HgBa_2CuO_{4+\delta}$ superconductor, for which the effect was attributed to the opening of the pseudo gap above the superconducting phase transition.[28]

Similarly to V_{res}, the change in f_{res} strongly depends on the modification of σ, and magnetic and electric permeability at the electromagnetic phase transitions. An increase in μ causes a reduction of f_{res}, which is clearly observed for the Gd sample. For NiCoMnIn single crystal, the effect of μ increase at temperatures below 295 K is much less pronounced than that caused by MFIT. The increase in f_{res} in the superconducting state for Nb and YBCO is governed by a change in σ and the Meissner effect.[11,25] The peculiar decrease in f_{res} when the temperature is decreased below 55 K may be attributed to vortex relaxation due to columnar defects.[29] Another unexpected result related to the behavior of f_{res} is its increase for V_2O_3 film in the insulating state [Fig. 4(c)]. Typically, an increase in resistivity causes a decrease in f_{res},[15] as found for another vanadium oxide, VO_2, which is undergoing metal-insulating transition at around 340 K. The unusual behavior of V_2O_3 may be attributed to the antiferromagnetism of V_2O_3 in the insulating state.[30,31] Hence, a rise of f_{res} at low temperatures may be due to suppression of μ rather than significant enhancement of σ.

Temperature is a crucial characteristic parameter of all of the above-mentioned phase transitions. To ensure reliable temperature reading, the thermometer was placed outside of the cavity in close proximity to the sample tube. Additionally, the cavity mass was minimized to limit the thermal inertia. All these precautions enable accurate temperature readings. At low temperatures, the temperature difference between the cryostat and on-cavity thermometers during a 0.5 K/min scan is less than 0.2 K. However, due to the heat capacitance of the cavity and the fact that heat exchange at the insert is provided by He exchange gas, the temperature difference may rise for higher temperature measurements (above 100 K). Based on the hysteresis of V_{res} (T) and f_{res} (T) curves, the inaccuracy of the readings does not exceed 1 K. The observed deviation of the measured phase-transition temperature from the nominal superconducting temperature for Nb is most probably related to the quality of the surface of the sample probed by the HC susceptometry (S.1 in the supplementary material). The enhanced temperature hysteresis observed for the V_2O_3 film may be related to the physical properties of the material.

V. CONCLUSION

The HC susceptometer we developed is an easy-to-implement apparatus that can be used as a powerful tool for detecting various phase transitions in different materials and qualitative analysis of electrical conductivity, and magnetic and electric permeability of materials in different phases. The complete design and control software is provided free by the authors, and any reproduction and further design improvements are highly encouraged. It is important to mention that certain modifications in the apparatus design can improve its sensitivity. First, it would be beneficial to use a gold-plated cavity to enhance the Q-factor and temperature drift of parameters for the unloaded HC. Second, the currently implemented software PLL control enables fine-tuning of the parameters; however, it is much slower than an electronic hardware PLL control. The ideal solution would be to implement a hybrid control for which an electronic module controls the PLL at a very high correction frequency; at the same time, the parameters of the control can be monitored and adjusted in software in real time.

Although the primary purpose of this manuscript was to demonstrate the capabilities of the apparatus, a few interesting observations were made. First, it was shown an unusual absorption hysteresis for a cavity with a NiCoMnIn single crystal at a temperature slightly above the martensite–austenite transition temperature. Additionally, MFIT yields significant modification of resonant parameters. Second, we observed enhanced absorption of the YBCO film below 55 K, which may be caused by modification of the superconducting vortices and could be used to study vortex dynamics in superconductors. Third, it was shown that simultaneous measurements of HC resonant voltage and frequency allow tracing not only change in electronic (metal–insulator) but also in magnetic (paramagnet–antiferromagnet) transitions of the V_2O_3 film.

SUPPLEMENTARY MATERIAL

The supplementary material contains the data illustrating the difference between the HC-susceptometer measurements conducted in the phase-locked and frequency-locked modes, and the Meissner-effect measurement of the Nb chip. The difference in the superconducting temperatures detected using the magnetometer and HC susceptometer is discussed.

ACKNOWLEDGMENTS

This research was supported by the National Science Foundation EAGER: SUPER: Light and Warm Superconducting Interfaces under Award No. 2132389.

The NiCoMnIn meta-magnetic shape memory alloys were fabricated by vacuum induction melting pure constituents. Single crystals were then grown via the Bridgeman method under a high-purity He environment by Professor Y. I. Chumlyakov at Tomsk State University.[22,32–35] High-quality epitaxial $YBa_2Cu_3O_7$ (100 nm) films were grown on $SrTiO_3$(100) substrate by Professor J. Santamaria's group at Universidad Complutense de Madrid.[36] V_2O_3 film was grown by the authors at the University of California, San Diego, using RF magnetron sputtering on top of an r-cut Al_2O_3 substrate.[37]

The authors would like to thank Dr. Nickolaus M. Bruno for helping with the magnetometry measurements, cutting the samples with wire EDM, supplying the samples, and for fruitful discussions about meta-magnetic phase transitions. Additionally, the

authors thank Alberto Rivera Calzada for his expertise regarding the properties of the YBCO superconductor.

AUTHOR DECLARATIONS

Conflict of Interest

The authors have no conflicts to disclose.

Author Contributions

Pavel N. Lapa: Conceptualization (equal); Data curation (equal); Formal analysis (equal); Investigation (lead); Methodology (equal); Software (equal); Validation (equal); Writing – original draft (lead). **George Kassabian**: Conceptualization (equal); Investigation (equal); Methodology (equal). **Ali C. Basaran**: Conceptualization (equal); Data curation (equal); Validation (equal); Visualization (equal); Writing – original draft (equal); Writing – review & editing (equal). **Ivan K. Schuller**: Conceptualization (equal); Data curation (equal); Formal analysis (equal); Funding acquisition (lead); Investigation (equal); Project administration (lead); Resources (equal); Supervision (lead); Validation (lead); Writing – review & editing (equal).

DATA AVAILABILITY

The data that support the findings of this study are available from the corresponding author upon reasonable request.

REFERENCES

[1]J. G. Ramírez, A. C. Basaran, J. de la Venta, J. Pereiro, and I. K. Schuller, Rep. Prog. Phys. **77**, 093902 (2014).
[2]N. Abhyankar, A. Agrawal, J. Campbell, T. Maly, P. Shrestha, and V. Szalai, Rev. Sci. Instrum. **93**, 101101 (2022).
[3]M. Yu and V. Dokas, in *34th European Microwave Conference* (Horizon House Publishers, 2004), Vol. **2**, pp. 989–992.
[4]J. Nandi, A. K. Sikdar, P. Das, and A. Ray, Rev. Sci. Instrum. **93**, 014706 (2022).
[5]S. J. Fiedziuszko and R. S. Kwok, in presented at the 1998 IEEE MTT-S International Microwave Symposium Digest (Cat. No.98CH36192), 1998.
[6]T. Guo, P. Liu, and C. Lee, Chin. Phys. B **31**, 093201 (2022).
[7]R. Benaroya, A. H. Jaffey, K. Johnson, T. Khoe, J. J. Livingood, J. M. Nixon, G. W. Parker, W. J. Ramler, J. Aron, and W. A. Wesolowski, Appl. Phys. Lett. **21**, 235–236 (1972).
[8]W. Meyer, IEEE Trans. Microwave Theory Tech. **29**, 240–247 (1981).
[9]R. Diehl, D. M. Wheatley, and T. G. Castner, Rev. Sci. Instrum. **67**, 3904–3913 (1996).
[10]D. R. Bowling, R. J. Dinger, and N. M. Alford, in presented at the International Symposium on Antennas and Propagation Society, Merging Technologies for the 90's, 1990.
[11]L.-Y. Chen and J.-T. Lue, Solid State Commun. **90**, 451–454 (1994).
[12]S. Guénon, J. G. Ramírez, A. C. Basaran, J. Wampler, M. Thiemens, S. Taylor, and I. K. Schuller, Sci. Rep. **4**, 7333 (2014).
[13]D. Yazici, A. C. Basaran, J. G. Ramírez, I. K. Schuller, and M. B. Maple, Supercond. Sci. Technol. **29**, 085015 (2016).
[14]P.-d.-J. Cuadra-Solís, A. Fernández-Martínez, J. M. Hernàndez, A. García-Santiago, J. Vanacken, and V. V. Moshchalkov, Rev. Sci. Instrum. **86**, 064701 (2015).
[15]J. Krupka and J. Mazierska, IEEE Trans. Instrum. Meas. **56**, 1839–1844 (2007).
[16]J. J. Rhyne, *Magnetic Properties of Rare Earth Metals*, edited by R. J. Elliott (Springer US, Boston, MA, 1972), pp. 129–185.
[17]H. E. Nigh, S. Legvold, and F. H. Spedding, Phys. Rev. **132**, 1092–1097 (1963).
[18]W. Ito, K. Ito, R. Y. Umetsu, R. Kainuma, K. Koyama, K. Watanabe, A. Fujita, K. Oikawa, K. Ishida, and T. Kanomata, Appl. Phys. Lett. **92**, 021908 (2008).
[19]H. E. Karaca, I. Karaman, B. Basaran, Y. Ren, Y. I. Chumlyakov, and H. J. Maier, Adv. Funct. Mater. **19**, 983–998 (2009).
[20]W. Ito, M. Nagasako, R. Y. Umetsu, R. Kainuma, T. Kanomata, and K. Ishida, Appl. Phys. Lett. **93**, 232503 (2008).
[21]R. Kainuma, Y. Imano, W. Ito, Y. Sutou, H. Morito, S. Okamoto, O. Kitakami, K. Oikawa, A. Fujita, T. Kanomata, and K. Ishida, Nature **439**, 957–960 (2006).
[22]N. M. Bruno, D. Salas, S. Wang, I. V. Roshchin, R. Santamarta, R. Arroyave, T. Duong, Y. I. Chumlyakov, and I. Karaman, Acta Mater. **142**, 95–106 (2018).
[23]H. W. Jackson and M. Barmatz, J. Appl. Phys. **70**, 5193–5204 (1991).
[24]S. Campione, I. C. Reines, L. K. Warne, C. Grimms, J. T. Williams, R. K. Gutierrez, R. S. Coats, and L. I. Basilio, Electron. Lett. **55**, 644–646 (2019).
[25]D.-N. Peligrad, B. Nebendahl, M. Mehring, A. Dulčić, M. Požek, and D. Paar, Phys. Rev. B **64**, 224504 (2001).
[26]J. Wampler, N. Hua, R. Kukreja, J. G. Ramírez, A. C. Basaran, E. E. Fullerton, O. Shpyrko, and I. K. Schuller, Phys. Rev. B **106**, L060402 (2022).
[27]H. A. Haus and J. R. Melcher, *Electromagnetic Fields and Energy* (Prentice Hall, Englewood Cliffs, 1989), Chap. 11.5.
[28]M. S. Grbić, N. Barišić, A. Dulčić, I. Kupčić, Y. Li, X. Zhao, G. Yu, M. Dressel, M. Greven, and M. Požek, Phys. Rev. B **80**, 094511 (2009).
[29]D. S. Fisher, M. P. A. Fisher, and D. A. Huse, Phys. Rev. B **43**, 130–159 (1991).
[30]R. M. Moon, J. Appl. Phys. **41**, 883 (1970).
[31]J. Trastoy, A. Camjayi, J. del Valle, Y. Kalcheim, J.-P. Crocombette, D. A. Gilbert, J. A. Borchers, J. E. Villegas, D. Ravelosona, M. J. Rozenberg, and I. K. Schuller, Phys. Rev. B **101**, 245109 (2020).
[32]N. Bruno, S. Wang, I. Karaman, and Y. Chumlyakov, Sci. Rep. **7**, 40434 (2017).
[33]P. J. Stonaha, I. Karaman, R. Arroyave, D. Salas, N. M. Bruno, Y. Wang, M. F. Chisholm, S. Chi, D. L. Abernathy, Y. I. Chumlyakov, and M. E. Manley, Phys. Rev. Lett. **120**, 245701 (2018).
[34]N. M. Bruno, I. Karaman, and Y. I. Chumlyakov, Phys. Status Solidi B **255**, 1700437 (2018).
[35]P. J. Stonaha, M. E. Manley, N. M. Bruno, I. Karaman, R. Arroyave, N. Singh, D. L. Abernathy, and S. Chi, Phys. Rev. B **92**, 140406 (2015).
[36]Z. Sefrioui, D. Arias, E. M. González, C. León, J. Santamaria, and J. L. Vicent, Phys. Rev. B **63**, 064503 (2001).
[37]J. Trastoy, Y. Kalcheim, J. del Valle, I. Valmianski, and I. K. Schuller, J. Mater. Sci. **53**, 9131–9137 (2018).